Thermal management of LED with vapor chamber and thermoelectric cooling

K.S. Ong[1,*], C.F. Tan[1], K.C. Lai[1], K.H. Tan[1], R. Singh[2]
[1]Faculty of Engineering and Green Technology, Universiti Tunku Abdul Rahman, Malaysia
[2]Fujikura Automotive Europe GmbH, Köln, Germany
*Email: skong@utar.edu.my

Abstract

A fin heat sink (FHS) is a thermal heat transfer device employed to dissipate heat from a high temperature heat source to a lower temperature surrounding. A typical FHS consists of a flat metal base with an array of cooling fins on top. A problem normally encountered in thermal management of electronic packages is thermal heat spreading resistance which occurs as heat flows by conduction from a high temperature heat source to a low temperature heat sink with different cross-sectional areas. As high powered semiconductor chips are made more compact and requiring greater heat dissipation, more effective cooling systems have to be devised. There are various methods employed to minimize this heat spreading resistance. These include increasing the thickness of the base of the FHS or height of the fins. Another method is to use more expensive highly conductive materials like aluminum, copper and diamond which would increase cost. A more economical alternative would be to combine a flat heat pipe (HP) sometimes termed a vapor chamber (VC) with a conventional FHS to increase effective thermal conductivity at the base. Thermoelectric (TE) is the direct conversion of temperature difference between the junctions of two dissimilar materials (thermocouple) to electricity. The converse is true. A voltage applied between the junctions of the thermocouple creates a temperature difference between them. This effect could be utilized as a heat pump to transfer heat from the cold junction to the hot junction. A dc voltage imposed across a thermoelectric (TE) module causes a temperature difference to be imposed across the surfaces of the resulting in one face to be at a temperature higher than the other face. Heat is absorbed from a heat source in contact with the cold surface and dissipated to a heat sink in contact with the hot surface. This paper presents the results of an investigation conducted to evaluate the performance of VCs and TEs for the thermal management of LEDs.

1. Introduction

Electronic components are normally cooled using a conventional fin heat sink (FHS) under natural (NC) or force convection (FC) cooling. A problem normally encountered in thermal management of electronic packages is thermal heat spreading resistance which occurs as heat flows by conduction from a high temperature heat source to a low temperature heat sink with different cross-sectional areas. Heat spreading resistance reduces the efficiency of the cooling device. As high powered semiconductor chips are made more compact they require greater heat dissipation. Hence, more effective cooling systems have to be devised. The performance and life span of a light emitting diode (LED) is affected by its operating temperature. The performance of a conventional FHS could be improved by incorporating a vapor chamber (VC) or thermoelectric (TE) module to it. The VC is a flat plate heat pipe (HP) device with very high heat transfer capability. A TE module produces hot and cold surfaces when a dc voltage is applied to it. The FHS-VC and FHS-TE assemblies are illustrated in Fig. 1. The objective of the present study would be to determine the experimental performance of these devices for efficient cooling of LEDs. The heat produced by the LEDs is simulated using electrical resistance heating elements.

Mochizuki et al. [1] presented an overview of the thermal management of high performance computers using HPs and VCs. Sauciuc et al. [2] theorised that there is a threshold envelope where a solid metal heat sink base may have lower thermal spreading resistance than a VC. A theoretical analysis by Lee et al. [3] showed that the constriction and spreading resistances for relatively thick plates were insensitive to plate thickness and Biot number. They were solely dependent upon relative contact size between heat sink and heat source. Simons [4] obtained results similar with that of Lee [3]. Ellison [5] derived three-dimensional solution to determine the maximum heat spreading resistance for rectangular heat sources centered on larger size plane heat sinks. Muzychka et al. [6] presented a general solution based on the separation of variables method for the thermal spreading resistances of eccentric heat sources on a rectangular flux channel. Tsai et al. [7] studied the thermal performance of a water-filled copper VC under both FC air and water cooling. They found that for the air-cooled VC thermal resistance was 0.51 K/W at 73 W and fill ratio of 0.34. For the water-cooled VC it was 0.18 K/W at 243 W. A decrease of about 42 % was obtained compared to using a normal heat sink alone. In a later paper, Tsai et al. [8] showed that thermal resistances decreased as power input increased and that spreading resistance dominated over the other resistances. They obtained a thermal resistance of 0.893K/W at 50 W. Wei et al. [9] showed that the VC in a horizontal position performed better than in the vertical position and also that the thermal heat spreading resistance across the VC was very small and may be neglected. At a heat flux of 43 W/cm^2, the thermal resistance of the VC was about 0.095 K/W for horizontal orientation and 0.110 K/W for vertical orientation. They compared their VC with copper and aluminum heat sinks and showed that a copper base heat sink performed close to that of the VC. They concluded that a VC base heat sink is useful for applications requiring large footprints such as for heat sinks in low profile servers and for systems requiring lower overall weight. Boukhanouf et al. [10] used a thermal imaging camera to compare performances of a working VC, a defective one and also with a solid copper block and showed that at 28 W/m^2, the spreading resistance was 0.0007K/W compared to a defective unit at 0.035K/W. Luo et al. [11] determined the performance of a 20 W LED light source cooled with a VC coupled fin heat sink and compared it with a conventional

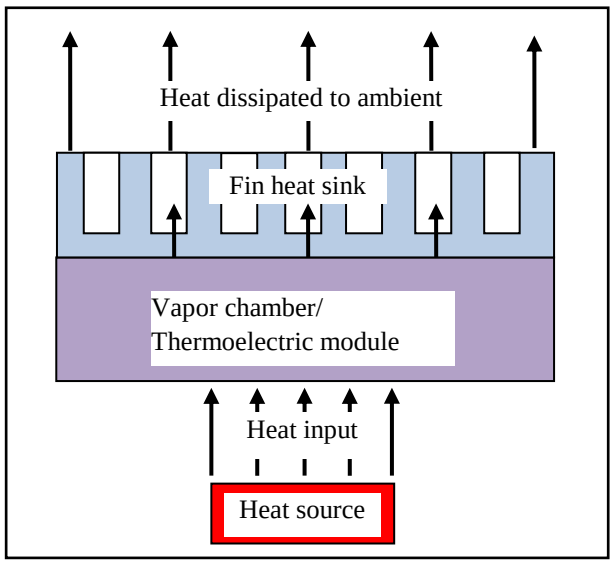

Fig. 1. Fin heat sink with VC/TE module.

FHS under FC air cooling conditions with an aspect ratio of 0.00044. They showed that the temperature at the bottom of the heat sink with the VC was quite uniform to within 0.4°C whereas a temperature difference of 2°C was obtained without the VC. At 20 W, they obtained values of 0.1165, 0.0555 and 0.4818 K/W for spreading, VC and fin resistances, respectively. Huang et al. [12] investigated the performances of a VC coupled to a FHS for LED cooling with an aspect ratio of 0.0004. They showed that at 30 W LED power input, the spreading resistance and corresponding temperature of the VC were lower than those of a copper plate by 34% and 4°C, respectively and 56% and 6°C compared to an aluminum plate. Oliveira et al. [13] machined the base off a conventional aluminum FHS and fitted a VC in its place. They found that the smallest resistance was obtained with 30% fill ratio at 200 W. The total experimental thermal resistance of the VC heat sink was 0.21 K/W compared to 0.24 K/W for the conventional one and that the VC was useful only at high heat inputs.

Koito et al. [14] proposed a spreading resistance based on the logarithmic mean temperature difference between the mean heat sink base temperature and the inlet and outlet air temperatures and found that it was substantially independent of power input while the thermal resistance of the VC increases with power input. Inclination did not affect the VC thermal resistance.

Glover et al. [15] compared the performances of various combinations of FHSs placed over the top of VCs or embedded with HPs at the base and showed that the best performances were obtained using the VC with sintered powder at the base (evaporator section) and wire-mesh at the sides and top (condenser section) of the VC. They concluded that the enhanced thermal performance, lighter weight and lower profile made the VC technology more attractive than conventional solid copper-base heat sinks.

Hsieh et al. [16] found a minimum filling ratio of about 0.275 was required to prevent system dry out. Huang [17] introduced a novel technology to produce a VC substrate printed circuit board that bonded an aray of LEDs to a VC to improve heat dissipation for LED lighting. Wei and Sikka [18] developed a thermal model and showed that the VC out-performed a copper heat sink when the footprint or aspect ratio between heat sink and heat source was small. Prasher [19] introduced a simplified modeling scheme for the prediction of heat transport capability of HPs and VC. He pointed out depending upon the configuration and the dimensions, a VC may perform better, equal or worse than a copper heat sink.

2. Experimental investigation of FHS

The thermal resistance network of a FHS is shown in Fig. 2. The aspect ratio (ε) is defined as the area of heat source/area of base of FHS. The temperature profile due to heat spreading effect is illustrated by varying ε from 0 – 1. The thermal resistances are calculated according:

Aluminium block:

$$R_{al} = \left(T_s - T_{alm}\right) / P_{EH} \tag{1}$$

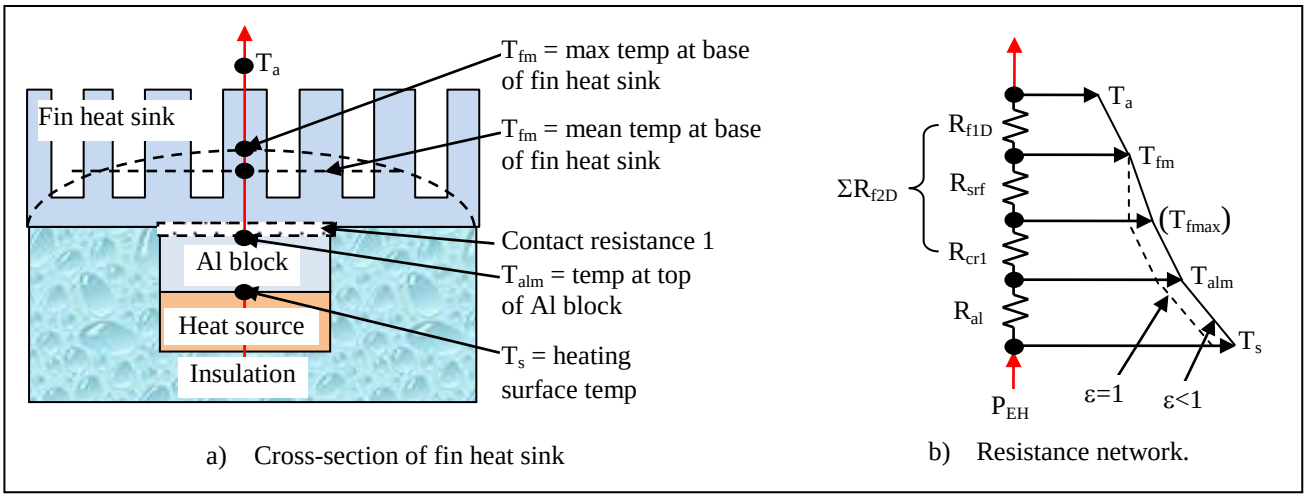

Fig. 2. Thermal resistance network of fin heat sink.

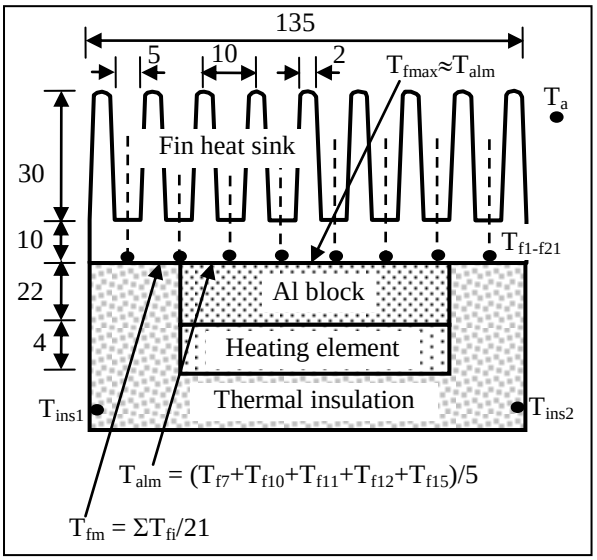

Fig. 3. Experimental FHS

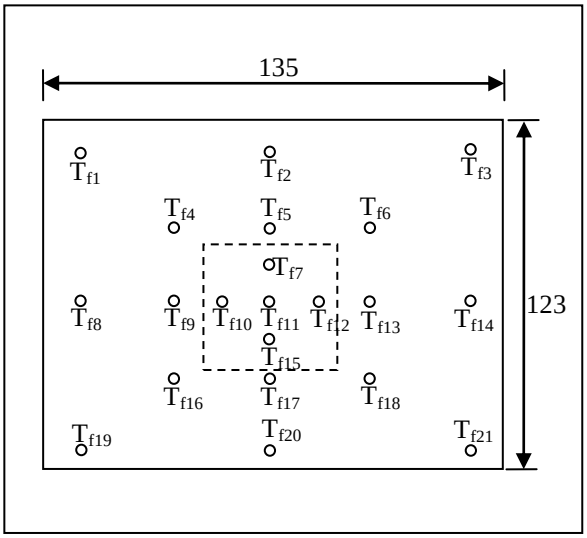

Fig. 4. Location of thermocouples on base of FHS

contact at the aluminum block/FHS interface:

$$R_{cr1} = (T_{alm} - T_{f\max}) / P_{EH} \quad (2)$$

heat spreading:

$$R_{srf} = (T_{f\max} - T_{fm}) / P_{EH} \quad (3)$$

1-D fin resistance:

$$R_{f1D} = (T_{fin} - T_a) / P_{EH} \quad (4)$$

total FHS resistance:

$$\sum R_f 2D = R_{cr1} + R_{srf} + R_{f1D} \quad (5)$$

or:

$$\sum R_f 2D = (T_{alm} - T_a) / P_{EH} \quad (6)$$

contact resistance of thermal interface material (TIM) between FHS and heat source:

$$R_{tim} = \Delta x_{tim} / k_{tim} \cdot A_{tim} \quad (7)$$

Table 1 Experimental results with FHS.

Run #	P_{EH} (W)	P_{EH}" (W)	T_a (°C)	$T_{alm}=T_{fmax}$ (°C)	T_{fm} (°C)	$R_{cr1}+R_{srf}$ (K/W)	R_{f1D} (K/W)	ΣR_{f2D} (K/W)
B1	10.1	1.1	20.8	37.8±0.3	36.9±1.0	0.09	1.59	1.68
	29.3	3.3	20.7	62.5±0.6	60.1±2.6	0.08	1.34	1.42
	50.4	5.6	20.9	84.3±1.2	80.1±4.3	0.08	1.17	1.25
B2	10.1	1.1	20.0	36.6±0.2	35.7±1.0	0.09	1.55	1.64
	29.9	3.3	20.4	62.0±0.7	59.5±2.6	0.08	1.31	1.39
	50.1	5.6	21.3	85.3±1.2	80.9±4.6	0.09	1.19	1.28
B3	10.0	1.1	19.8	35.1±0.3	34.3±1.0	0.08	1.45	1.53
	29.8	3.3	20.4	61.2±0.6	58.7±2.6	0.08	1.29	1.37
	50.1	5.6	20.4	84.1±1.2	79.8±4.6	0.09	1.19	1.28

An experimental investigation was conducted to determine the thermal performance of a conventional FHS under NC air cooling, Fig. 3. The FHS was 135 mm wide by 123 mm long and the heating element measured 30 x 30 mm x 4 mm thick (ε = 0.053). A 22 mm thick aluminum block was employed to minimize the effect of non-uniform heating from the heating element. Twenty one holes drilled from the top of the FHS through to its base allowed thermocouples (T_{f1-21}) to be inserted, Fig. 4. The mean bottom surface temperature (T_{fm}) of the FHS was calculated from the arithmetic average of these thermocouples. The surface temperature (T_{alm}) at the top of the aluminum block was assumed uniform and calculated based on the arithmetic average of the 5 thermocouples (T_{f7}, T_{f10}, T_{f11}, T_{f12} and T_{f15}). In theory, heat spreading effect could cause T_{alm} to be non-uniform. The contact resistance (R_{cr1}) was estimated at about 0.05 K/W based on manufacturer's specifications. The maximum temperature at the bottom of the FHS (T_{fmax}) was assumed equal to the mean surface temperature (T_{alm}). Other thermocouples measured the insulation surface temperature ($T_{ins1,}$ T_{ins2}) and the ambient temperature (T_a). Ambient temperature was not kept constant and varied from about 19.8 – 21.3°C. Experiments were performed at three power inputs from 10 – 50 W under NC air cooling with the FHS placed in a horizontal position. Three separate runs were conducted over a period of 2 hours each to determine experimental repeatability. The results are tabulated in Table 1.

The following results were obtained:

- High power input (P_{EH}) resulted in higher temperatures as expected.
- Heat flux ranged from 1.1 to 5.6 W/cm^2.
- Temperature (T_{fm}) at the base of the FHS varied by up to 4.6°C at high power input due to thermal heat spreading.
- Temperature distribution on the top surface of the aluminum block (T_{alm}) varied up to 1.2°C at high power input due to thermal heat spreading here.

- The present experimental results combined the thermal heat spreading resistance (R_{srf}) with the contact resistance (R_{cr1}) because the thermocouples were in contact with the top surface of the aluminum block. The combined thermal resistance was about 0.08 - 0.09 K/W. However, because of the small temperature difference (T_{alm}-T_{fm}) the determination of the resistance from Eqs. (2) and (3) could vary by as much as $\pm$ 0.1 K/W.
- The FHS was very efficient in removing heat.
- The present heat flux is small, 5.6 W/cm^2 at 50 W. The experiment could be extended to include higher heat flux, up to 100 W/cm^2 in line with increased demand for higher cooling capacity.
- The 1-D fin thermal resistance (R_{f1D}) decreased from about 1.59 K/W at low power to 1.17 K/W at high power owing to higher natural convection heat transfer coefficient between the FHS and ambient as a result of higher FHS temperature.
- The total heat spreading resistance of the FHS (ΣR_{f2D}) decreased from about 1.68 K/W at low power input to 1.25 K/W at high power.

3. Experimental investigation of FHS-VC system

The thermal resistance network of a FHS with VC is shown in Fig. 5. The aspect ratio (ε) is defined as the area of heat source/area of base of VC. Thermal contact resistances (R_{cr2} and R_{cr3}) are shown at the VC-FHS and the VC-aluminum block interfaces. The temperature profile due to heat spreading effect at the interface between bottom of the VC and the aluminum block is illustrated by varying ε from 0 – 1. The surface temperature (T_{vctop}) at the top of the VC is assumed uniform. Thermal heat spreading occurs at the interface between the bottom of the VC and the top of the aluminum block. As a result, there is a maximum temperature (T_{vcmax}) and a mean temperature (T_{vcbot}) at the bottom surface of the VC.

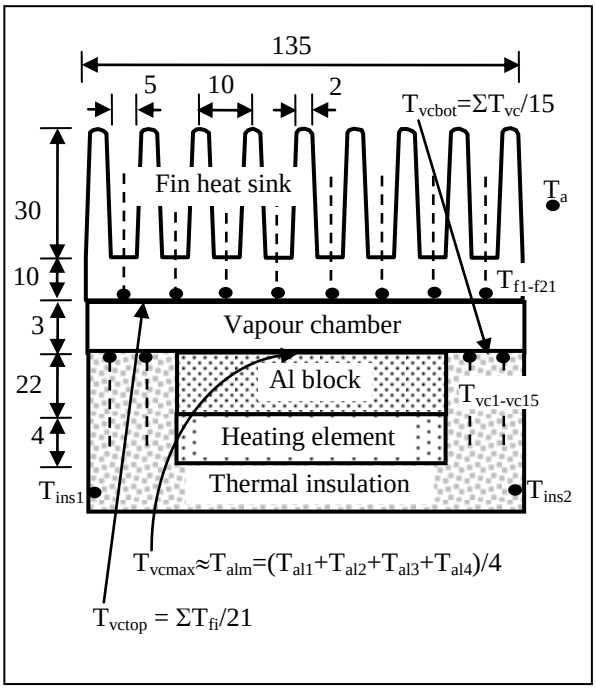

Fig. 6. Experimental FHS-VC assembly.

The thermal resistances are calculated according:
Contact resistances:

$$R_{cr2} = (T_{alm} - T_{vc\max})/P_{EH} \quad (8)$$

$$R_{cr3} = (T_{vctop} - T_{fm})/P_{EH} \quad (9)$$

heat spreading resistance at base of the VC:

$$R_{srvc} = (T_{vc\max} - T_{vcm})/P_{EH} \quad (10)$$

resistance of the VC:

$$R_{vc} = (T_{vcbot} - T_{vctop})/P_{EH} \quad (11)$$

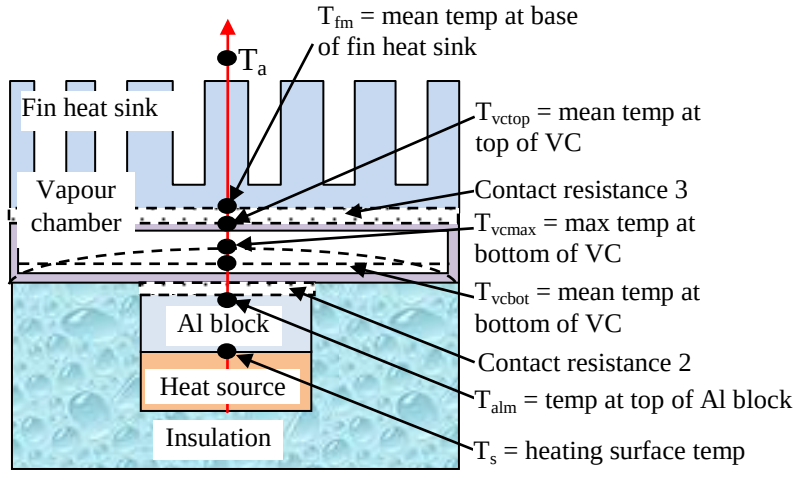

a) Cross-section of FHS-VC system.

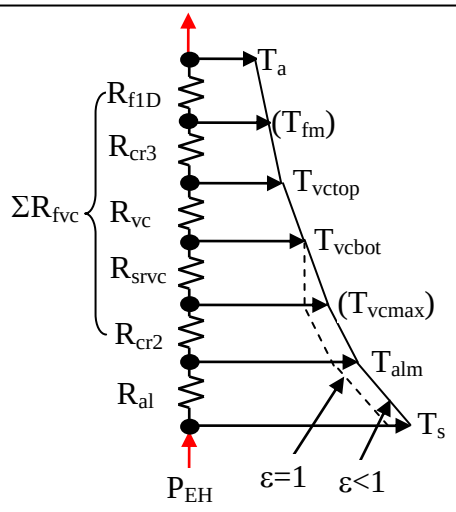

b) Resistance network of FHS-VC system

Fig. 5. Thermal resistance network of FHS-VC system.

Table 2 Experimental results with FHS-VC system.

Run #	P_{EH} (W)	T_a (°C)	T_{alm} (°C)	T_{vcbot} (°C)	T_{vctop} (°C)	$R_{f1D}+R_{cr3}$ (K/W)	R_{vc} (K/W)	ΣR_{f2D} (K/W)	ΣR_{fvc} (K/W)
C1	10.0	20.6	41.1±0.3	37.9±2.1	37.8±0.4	1.72	0.01	1.68	2.10
	29.9	20.5	69.2±0.7	60.7±5.5	60.1±0.6	1.32	0.02	1.42	1.62
	49.9	21.0	95.7±0.9	81.8±9.3	79.6±0.8	1.17	0.04	1.25	1.49
C2	10.0	19.8	38.6±0.3	35.6±2.1	35.5±0.4	1.57	0.01	1.64	1.94
	29.8	20.3	68.2±0.7	59.6±5.5	59.1±0.6	1.30	0.02	1.39	1.61
	50.2	20.8	97.4±1.0	82.0±9.8	79.8±1.0	1.18	0.04	1.28	1.53
C3	10.1	20.0	40.7±0.3	37.5±2.2	37.4±0.5	1.72	0.01	1.53	2.10
	29.8	20.3	68.9±0.6	60.2±5.5	59.6±0.6	1.32	0.02	1.37	1.63
	50.1	20.4	96.4±0.9	81.6±9.4	79.5±0.9	1.18	0.04	1.28	1.52

overall resistance of the FHS-VC assembly:

$$\sum R_{fvc} = R_{cr2} + R_{srvc} + R_{vc} + R_{cr3} + R_{f1D} \quad (12)$$

or:

$$\sum R_{fvc} = (T_{alm} - T_a)/P_{EH} \quad (13)$$

An experimental investigation was carried out to determine the thermal performance of a conventional aluminum FHS attached to a VC of near similar size under NC air cooling as shown in Fig. 6. The VC measured 139 x 123 wide x 3 mm thick. The FHS measured 135 x 123 mm with 13 fins. The heating element measured 30 x 30 x 4 mm thick and the aluminum block measured 30 x 30 x 22 mm thick. The aspect ratio (ε) of heating element/VC was 0.053. Thermal heat spreading effects are expected at the bottom of the VC with this arrangement especially a high input power. Twenty one type-T thermocouples ($T_{f1\text{-}f21}$) were inserted through holes drilled into the FHS to measure the temperature distribution at the interface between the bottom of the FHS and the top surface of the VC. The mean surface temperature of the top surface of the VC (T_{vctop}) was calculated from the arithmetic average of these twenty one thermocouples.

Four thermocouples ($T_{al1\text{-}al4}$) were inserted into grooves machined on the top surface of the aluminum block. The mean surface temperature of the top of the aluminum block (T_{alm}) was determined from the arithmetic mean of these four thermocouples. Another 15 thermocouples ($T_{vc1\text{-}vc15}$) were inserted through the bottom thermal insulation were used to measure the mean bottom surface temperature(T_{vcbot}) of the VC represented by the arithmetic mean of these 15 probes. It was not possible to probe through the heating element. Hence the maximum temperature at the bottom of the VC (T_{vcmax}) was assumed to be equal to T_{alm}. Other thermocouples measured the insulation surface temperatures (T_{ins1} and T_{ins2}) and the ambient temperature (T_a). Experiments were performed at three power inputs from 10 – 50 W under natural convection air cooling with the FHS in a horizontal position. Each run was conducted three times (Runs C1 – C3) for repeatability and over a period of a few hours to reach steady state. Thermal resistances (R_{f1D} + R_{cr3}), R_{vc}, (R_{cr2} + R_{srvc}) and the overall thermal resistance of the FHS-VC assembly (ΣF_{fvc}) are calculated and tabulated in Table 2. Ambient temperature was not controlled and varied from 19.8 - 21.0°C. From the insulation temperature results, heat loss from the sides accounted for about 2% at the low power input to less than 0.2% at the higher power input.

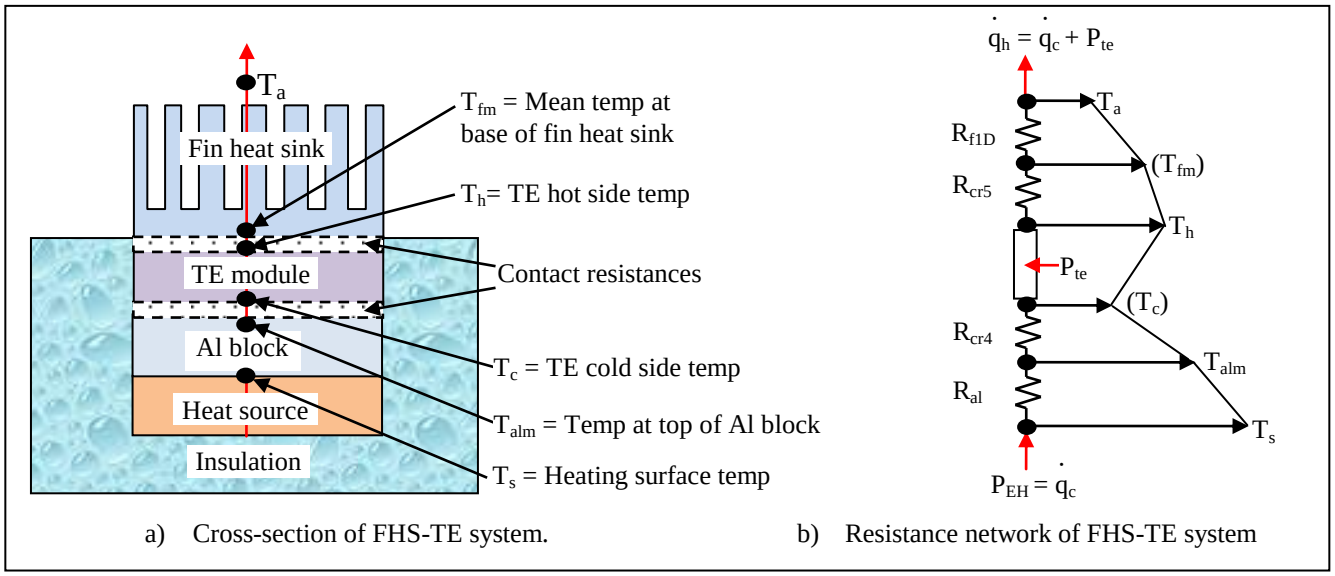

Fig. 7. Thermal resistance network of FHS-TE system.

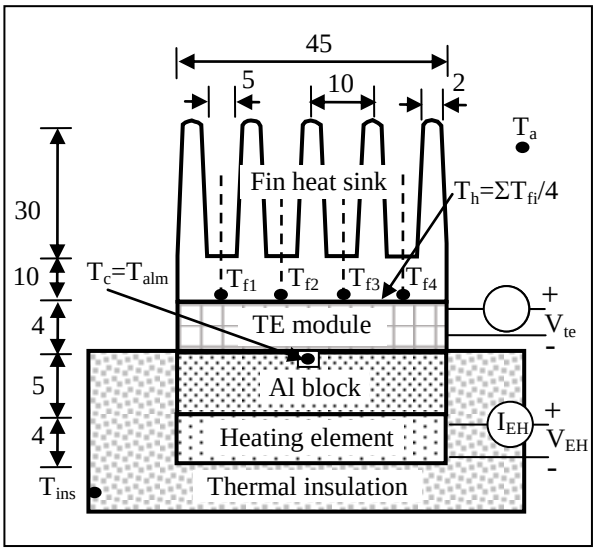

Fig. 8. Experimental FHS-TE assembly.

Overall, the results were repeatable to within 3°C.
The following conclusions can be reached:

- High power input (P_{EH}) results in higher temperatures as expected.
- Temperature at the bottom of the VC (T_{vcbot}) varied from about 2.1°C at low power to 9.8°C at high power showing the effects of thermal heat spreading at the interface here.
- Temperature at the top of the VC (T_{vctop}) was quite uniform, (< 1°C) showing the effectiveness of the VC to spread out the heat evenly.
- The thermal heat spreading resistance at the bottom of the VC including the thermal contact resistance (R_{cr2} + R_{srvc}) was about 0.28 - 0.37 K/W.
- The thermal resistance of the VC (R_{vc}) was very small, 0.01 - 0.04 K/W.
- The thermal resistance of the FHS at the top of the VC including the thermal contact resistance (R_{cr3} + R_{f1D}) decreased with power input 1.72 – 1.17 K/W.
- The total thermal resistance of the FHS-VC assembly ($\sum R_{fvc}$) decreased with power input and varied from 2.10 – 1.49 K/W.

4. Experimental investigation of FHS-TE system

The thermal resistance network for the FHS-TE assembly is shown in Fig. 7. The aspect ratio for this case is ε = 1 as the TE is employed only to provide a cold surface and not to reduce thermal heat spreading. All interface temperatures are expected to be uniform since the heat flow is 1-dimensional. A voltage (V_{te}) and current (I_{te}) supplied to the TE module creates a temperature difference (ΔT_{te}) across the TE with TE hot side (T_h) temperature greater than the cold side (T_c). Assuming perfect insulation with no heat loss, heat transfer rate (q_c) at the cold side is equal to the power supplied (P_{EH}) to the heater.

Heat dissipated to the ambient at the hot surface is given by:

$$q_h = q_c + P_{te} \tag{14}$$

The temperature difference across the TE module is:

$$\Delta T_{te} = T_h - T_c \tag{15}$$

The power supplied to the TE module is calculated by:

$$P_{te} = I_{te} V_{te}$$

The cooling coefficient of performance of the TE is:

$$COP_c = P_{EH} / P_{te} \tag{17}$$

An experimental assembly consisting of a FHS, TE module, aluminum block and heating element were clamped with a G-clamp as shown in Fig. 8. The FHS measured 45 mm x 45 mm x 10 mm thick base with 5 fins. The heating element measured 40 mm x 40 mm x 4 mm and the aluminum block 40 mm x 40 mm x 5 mm. The TE module used was Laird Technologies HT8,12,F2,4040. Thermal insulation was provided at the bottom and sides of the assembly up to and including the TE module to minimise heat loss to the ambient. The insulation consisted of a composite layer of 10 mm thick cork board and 95 mm thick rockwool. Heating was provided from an AC power supply. Power input (P_{EH}) was determined from the AC voltmeter (V_{EH}) and ammeter (I_{EH}) readings. Four thermocouples (T_{f1} - T_{f4}) inserted through holes drilled in a row through the heat sink measured the interface temperature between the base of the heat sink and the TE module.

Table 3 Experimental results with FHS-TE system.

Run #	P_{EH} (W)	V_{te} (V)	I_{te} (A)	P_{te} (W)	ΣP (W)	T_a (°C)	T_{ins} (°C)	$T_c=T_{alm}$ (°C)	T_h (°C)	ΔT_{te} (°C)	T_m (°C)	$R_{f1D}+R_{cr5}$ (K/W)	COP_c
D1	5.0	1.97	0.77	1.52	6.52	19.9	22.4	46.9	57.5	10.6	52.2	5.77	3.3
		3.98	1.40	5.57	10.57	18.7	21.1	52.5	75.1	22.6	63.8	5.34	0.9
		6.09	1.95	11.88	16.88	18.9	21.1	66.5	101.4	34.9	84.0	4.89	0.4
D2	7.5	1.99	0.77	1.53	9.03	19.8	21.9	58.3	66.8	8.5	62.6	5.20	4.9
		4.12	1.44	5.93	13.43	18.4	21.1	62.8	85.3	22.5	74.1	4.98	1.3
		6.14	1.97	12.10	19.60	20.1	22.4	78.3	111.4	33.1	94.9	4.66	0.6
D3	10.4	2.01	0.75	1.51	11.91	18.8	19.6	68.5	74.5	6.0	71.5	4.68	6.9
		4.02	1.31	5.27	15.67	20.7	21.0	76.1	94.2	18.1	85.2	4.69	2.0
		6.03	1.82	10.97	21.37	21.8	21.8	86.5	115.1	28.6	100.8	4.37	0.9
A	10.0	-				19.5	21.2	78.0	-			5.80	-

TE hot surface temperature (T_h) was obtained from the arithmetic mean of these four temperatures. A thermocouple centrally located in a 1.5 mm deep groove machined on the top surface of the aluminum block measured the mean surface temperature of the top of the aluminum block (T_{alm}). TE cold junction temperature (T_c) was assumed equal to T_{alm}. The mean operating temperature (T_m) across the TE module was calculated from the arithmetic mean temperature between hot (T_h) and cold surfaces (T_c). Additional thermocouples measured the external surface temperature of the insulation (T_{ins}) and ambient temperature (T_a). All thermocouples were connected to a data logger and logged every minute. Experiments were performed at heater power inputs between 5 – 10 W. The results are tabulated in Table 3 (Runs D1-D3).

The following results are obtained:

(a) All temperatures increased with electrical heating power input as expected.
(b) $COP_c > 1.0$ was obtained at low power input and at low TE current input.
(c) $COP_c < 1.0$ was obtained at high TE current input.
(d) In order to be effective, the TE should be operated when TE power input (P_{te}) < heat source power (P_{EH}).

5. Conclusions

The results of an experimental investigation conducted to evaluate the performances of vapor chamber and thermoeletric for the thermal management of LEDs were presented with the LED heat output substituted with electrical heating element. VCs are not effective at low heat input and high aspect ratio. Incorporating TE for cooling can reduce the surface temperature provided that the TE and heat sink are correctly selected.

Acknowledgments

The study was funded by CREST, Malaysia and supported by OSRAM Opto Semiconductors, Malaysia.

References

1. Mochizuki, M., Mashiko, K., Saito, Y., Nguyen, T., Wu, X. P., Nguyen, T., Wittijumnong, V., "Thermal management in high performance computers by use of heat pipes and vapor chambers," *Proc. 9IHPS*, Malaysia, 2008, pp. 39-48.
2. Sauciuc, I., Chrysler, G., Mahajan, R., Prasher, R., Thermal Challenges in Next Generation Electronic Systems, Millpress (Rotterdam, 2002), pp. 211-220.
3. Lee, S., Song, S., Au, V., Moran, K. P., "Constriction/spreading resistance model for electronic packaging," *Proc. ASME/JSME Engineering Conference*, 1995, pp. 199-206.
4. Simons, R. E., "Simple formulas for estimating thermal spreading resistance," *Electronics Cooling Magazine*, 2004.
5. Ellison, G. N., "Maximum thermal spreading resistance for rectangular sources and plates with nonunity aspect ratios," *IEEE Trans. Components and Packaging Technologies*, Vol. 26, No. 2 (2003), pp. 439-454.
6. Muzychka, Y. S., Culham, J. R., Yovanovich, M. M., "Thermal spreading resistance of eccentric heat sources on rectangular flux channels," *Trans. ASME*, Vol. 125 (2003), pp. 178-185.
7. Tsai, M. C., Chien, K. C., Huang, C. Y., Kang, S. W., "Thermal performance of a vapor chamber," *Proc. 9IHPS*, Malaysia, 2008.
8. Tsai, M. C., Kang, S. W., Paiva, K. V., "Experimental studies of thermal resistance in a vapor chamber heat spreader," *Applied Thermal Engineering*, Vol. 56 (2013), pp. 38-44.
9. Wei, J., Chan, A., Copeland, D., "Measurement of vapor chamber performance," *19th IEEE Semi-Therm Symposium*, 2003, pp. 191-194.
10. Boukhanouf, R., Haddad, A., North, M. T., Buffone, C., "Experimental investigation of a flat plate heat pipe performance using a IR thermal imaging camera," *Applied Thermal Engineering*, Vol. 26 (2006), pp. 2148-2156..
11. Luo, X., Hu, R., Guo, T., Zhu, X., Chen, W., Mao, Z., Liu, S., "Low thermal resistance LED light source with vapor chamber coupled fin heat sink," *IEEE Electronic Components and Technology Conference*, 2010, pp. 1347-1352.
12. Huang, H. S., Chiang, Y. C., Huang, C. K., Chen, S. L., "Experimental investigation of vapor chamber module applied to high-power light-emitting diodes," *Experimental Heat Transfer*, Vol. 22 (2009), pp. 26-38.
13. Oliveira, A. S., Mantelli, M. B. H., Milanez, F. H., "Use of vapor chamber on electronic devices to eliminate hot spots under fin heat sinks," *Proc. 14th IHPC*, Brazil, 2007.
14. Koito, Y., Motomatsu, K., Imura, H., Mochizuki, M., Saito, Y., "Fundamental investigations on heat transfer characteristics of heat sinks with a vapor chamber," *Proc. 7IHPS*, Korea, 2003.
15. Glover, G., Chen, Y., Luo, A., Chu, H., "Thin vapor chamber heat sink and embedded heat pipe heat sink performance evaluations," *25th IEEE Semi-Therm Symposium*, 2009, pp. 30-37.
16. Hsieh, S. S., Lee, R. Y., Shyu, J. C., Chen ,S. W., "Thermal performance of flat vapor chamber heat spreader," *Energy Conversion & Management*, Vol. 49 (2008), pp. 1774-1784.
17. Huang, Z., Cheng, Z., Wu, M., "Heat dissipation for LED lighting: Vapor chamber substrate printed circuit board," *5th IEEE Conference on Industrial Electronics and Applications*, 2010, pp. 565-570.
18. Wei, X., Sikka, K., "Modeling of vapor chamber as heat spreading devices," *IEEE Conference on Thermal and Thermomechanical Phenomena in Electronics Systems*, 2006, pp. 578-584.
19. Prasher, R. S., "A simplified conduction based modeling scheme for design sensivity study of thermal solution utilizing heat pipe and vapor chamber technology," *Trans. ASME*, Vol. 125 (2003), pp. 378-385.